Nonstationary Langevin equation: Statistical properties and application to explain effects observed in cardiological time series

Jens Kirchner,* Wolfgang Meyer, Markus Elsholz, and Bernhard Hensel
Max Schaldach-Stiftungsprofessur, Center for Medical Physics and Engineering, Friedrich-Alexander-Universität Erlangen-Nürnberg, Germany
(Received 2 October 2006; revised manuscript received 15 May 2007; published 16 August 2007)

Using the Langevin equation we develop the model of a stochastic process subject to a given time-dependent regulatory mechanism. The effects of this nonstationarity on the statistical properties of the time series, i.e., on global and conditional probability densities and on the moments of the distribution, are derived. Application of these results on simple model trends allows one to approximate cardiological data and thus to explain effects recently observed in the reconstruction of the deterministic part of the Langevin equation for time series of heart rate.

DOI: 10.1103/PhysRevE.76.021110 PACS number(s): 05.40.−a, 05.10.Gg, 05.45.Tp, 87.19.Hh

I. INTRODUCTION

The human cardiovascular system as an open system is subject to varying environmental influences, which it has to adapt to in order to maintain the vital functions of the organism. Measured cardiological signals and time series of the RR intervals, i.e., of the distance between successive R peaks in the ECG, in particular are thus a superposition of deterministic reactions of the system to this changing input from the environment on a variety of time scales, as well as of noise sources within the body itself. Hence, in 24-h recordings of heart rate particularly circadian variation reflects different exposures of the body during day and night (see Figs. 1 and 2) [1,2]. Methods for extracting the parameters of such oscillatory behavior have been presented by Nelson *et al.* [3] and for more complex trends by Fernández and Hermida [4].

However, while the long-range behavior of the cardiovascular system, such as 24-h oscillations or phases of physical activity, can typically be related to the patient's specific activity, splitting heart rate into a deterministic and a stochastic part on small time scales is feasible only in rare cases such as respiratory oscillations. In order to model such time series, an equation of motion is hence needed comprising terms that represent deterministic regulations as well as noise sources. This purpose is served by the Langevin equation.

Conceived for describing the motion of a Brownian particle [5] the original equation more generally covers stochastic processes with linear damping [6,7]. In the so-called "Langevin approach" [8] the model is extended to include also the cases of nonlinear deterministic forces with additive noise. Using the definitions of a stochastic integral proposed by Itô [9] and Stratonovich [10] the Fokker-Planck equation of the process can be derived from the Langevin equation [8,11]. A further generalization of the model was achieved by admitting memory effects in the deterministic force [12–15]. Sometimes the name is even attributed to the whole class of processes including a stochastic force [7].

In this article we restrict ourselves to the case of a δ-correlated noise source. We will show that we are able to choose delay parameters in our model such that this simplification is applicable to the cardiovascular time series under examination. Furthermore, for this model, algorithms for reconstructing the drift and diffusion coefficients of the Fokker-Planck equation [16] as well as the coordinate-dependent functions in the Langevin equation [17] have been proposed and applied to a variety of synthetic and empirical data [18,19]. In particular, Kuusela *et al.* [20,21] as well as Ghasemi and co-workers [22] have recently used this method for the analysis of RR interval time series and have found characteristic differences in the shape of the reconstructed functions between healthy patients and those suffering from congestive heart failure.

Most publications basing on the Langevin equation limit their scope to stationary processes. From the considerations above, however, it is obvious that this assumption does not hold for time series of the cardiovascular system in general (see also Refs. [23–25]). Instead we have to model these signals as the result of a regulatory mechanism responding to changing stress or, relocating the nonstationarity into the adaptation mechanism itself and thus omitting to explicitly predefine an input signal, as the product of a time-varying regulation.

We therefore regard the signal under examination as following a time-dependent trend $\gamma(t)$. From the assumed antagonism between noise source and regulation on the target value γ, we derive the special form of the Langevin equation used for the subsequent analysis. The statistical properties of this model, i.e., the probability densities and the moments of the distribution are then calculated. In the second half of this article we use these results to demonstrate the effects on the algorithm mentioned above, if a process subject to time-varying regulation is treated as stationary: By analyzing the special case of a piecewise linear trend, we relate the two stable fixed points that were observed in cardiological data by Kuusela to distinct phases of constant physical stress, in particular during day and night.

*kirchner@biomed.uni-erlangen.de

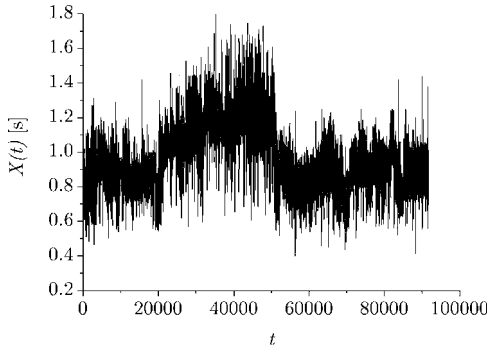

FIG. 1. 24-h time series of RR intervals $X(t)$ over beat number t.

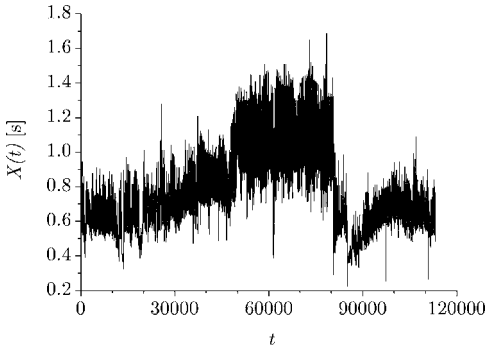

FIG. 2. 24-h time series of RR intervals $X(t)$ over beat number t.

II. MODEL

In order to develop the model used in this article we start from the Langevin equation as given by Risken [26],

$$\frac{dX(t)}{dt} = g[X(t),t] + h[X(t),t]\Gamma(t), \tag{1}$$

where the force g represents the deterministic mechanisms acting on $X(t)$. $\Gamma(t)$ is a stochastic process with zero correlation time, the amplitude of which is modulated by h.[1] Equation (1) is the most general form of a stochastic process with additive and δ-correlated noise $\Gamma(t)$; in comparison to Refs. [8,9,11,16–21] g and h additionally contain an explicit time dependency.

For the treatment of RR interval time series it has to be taken into account that $X(t)$ varies discretely with heart beat number. Hence, Eq. (1) has to be discretized by introducing a delay time τ [20,21]

$$X(t+\tau) - X(t) = g[X(t),t,\tau] + h[X(t),t]\Gamma(t,\tau), \tag{2}$$

where the form of the equation remains unchanged. For the application of our model to cardiological data it follows that both t and τ are positive integers, although the subsequent considerations will remain correct even for real-valued t and τ.

For the regulatory component represented by g we now assume a time-dependent set point $\gamma(t)$. In case of zero stochastic influences ($h \equiv 0$), $g[X(t),t,\tau]$ acts on X in such a way that $X(t+\tau)$ is set to the target value $\gamma(t+\tau)$, i.e. $X(t+\tau)=\gamma(t+\tau)$ for all $X(t)$. With Eq. (2) it follows that

$$g[X(t),t,\tau] = \gamma(t+\tau) - X(t). \tag{3}$$

Inserting g back into Eq. (2), now admitting stochastic influences, gives

$$X(t+\tau) = \gamma(t+\tau) + \Gamma(t,\tau), \tag{4}$$

where we have set $h \equiv 1$ for mathematical simplicity.[2] Then $X(t)$ is a linear combination of the two variables $\gamma(t)$ and $\Gamma(t,\tau)$, which are independent of each other. This fact will allow us to express the probability density of the process $X(t)$ in terms of the densities $\rho_\gamma(x)$ and $\rho_\Gamma(x)$ that are associated to the individual processes of the trend and the noise source.

Equation (4) will serve as model in the subsequent analysis. Thereby the following notation will be used: The signal $X(t)$ is observed during a time interval $I_t=[0,T]$. For $t \in I_t$, $\gamma(t)$ varies continuously within $I_\gamma=\gamma(I_t)=[\gamma_{\min},\gamma_{\max}]$.

III. PROBABILITY DENSITIES

In order to derive the statistical properties of $X(t)$, both components $\gamma(t)$ and $\Gamma(t,\tau)$ of the signal are treated as stochastic processes with associated probability densities $\rho_\gamma(x)$ and $\rho_\Gamma(x)$.

A. Global probability density

With X regarded as the sum of the two independent random variables γ and Γ its probability density $\rho(x)$ directly follows [27]

$$\rho(x) = \rho[\gamma(t) + \Gamma(t-\tau,\tau)] = [\rho_\gamma * \rho_\Gamma](x), \tag{5}$$

where

$$[\rho_\gamma * \rho_\Gamma](x) = \int_{-\infty}^{\infty} \rho_\gamma(s)\rho_\Gamma(x-s)ds \tag{6}$$

denotes the convolution of the probability densities of the individual processes.

It is then easy to show (see Appendix A) that the moments of X

[1]The following considerations aim at processes with Gaussian probability density $\rho_\Gamma(x)$, as is often assumed for Langevin processes, but are applicable to more general ρ_Γ. Additional constraints will be given, if needed, at the respective positions in the text.

[2]In order to take into account the increase of heart rate variability with mean heart rate [1] due to the raised sympathetic tone [implying $h=h(\gamma)$], $X(t)$ has to be rescaled by dividing Eq. (4) by $h(\gamma)$. In this case $\frac{\partial h(x)}{\partial x} < 0$ ensures $\frac{\partial}{\partial x}\frac{x}{h(x)} > 0$, so that the change of variables $x \to \frac{x}{h(x)}$ is bijective.

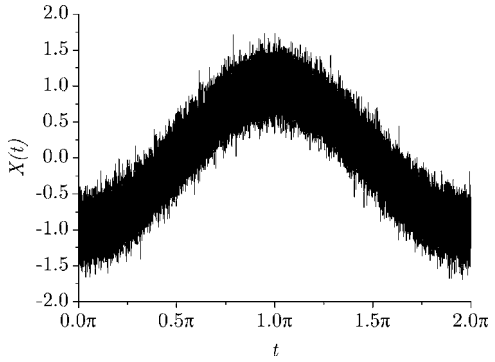

FIG. 3. Time series $X(t)$ of the cosine-shaped trend (13) ($A=-1$, $\omega=1$) with superimposed white noise ($\sigma=0.2$).

$$\langle X^n\rangle \equiv \int_{-\infty}^{\infty} x^n \rho(x)dx \tag{7}$$

can be related to the the moments of $\gamma(t)$ and $\Gamma(t,\tau)$,

$$\langle \gamma^n\rangle \equiv \int_{-\infty}^{\infty} x^n \rho_\gamma(x)dx, \tag{8}$$

$$\langle \Gamma^n\rangle \equiv \int_{-\infty}^{\infty} x^n \rho_\Gamma(x)dx, \tag{9}$$

by the following equation:

$$\langle X^n\rangle = \sum_{k=0}^{n} \binom{n}{k} \langle \gamma^k\rangle \langle \Gamma^{n-k}\rangle. \tag{10}$$

In order to determine $\rho_\gamma(x)$ from an analytically given, continuous $\gamma(t)$, it is required that for every interval J the corresponding probability $P\{\gamma(t)\in J\}$ for $\gamma(t)$ to be found in J is given by the length of time, when $\gamma(t)$ varies within J. From this it is derived that

$$\rho_\gamma(x) = \frac{1}{\|I_t\|} \left| \left[\frac{d}{ds} \gamma^{-1}(s) \right]_{s=x} \right| \tag{11}$$

for monotone $\gamma(t)$ and

$$\rho_\gamma(x) = \frac{1}{\|I_t\|} \sum_{k:x\in I_\gamma^{(k)}} \left| \left[\frac{d}{ds} \gamma_k^{-1}(s) \right]_{s=x} \right| \tag{12}$$

in the general case (see Appendix B). Here $I_t=\cup_k I_t^{(k)}$ is the sampling interval, which is split up into disjoint subintervals such that $\gamma(t)$ is monotone on each $I_t^{(k)}$ with value set $I_\gamma^{(k)}=\gamma(I_t^{(k)})$. Then $\gamma_k^{-1}(x)$ is the inverse of the bijection $\gamma(t)$ on $I_t^{(k)}$. Equation (12) implies for piecewise defined $\gamma(t)$ on I_t that $\rho_\gamma(t)$ is constituted by the average of the densities on each subinterval.

B. Applications

As an example consider the cosine-shaped trend

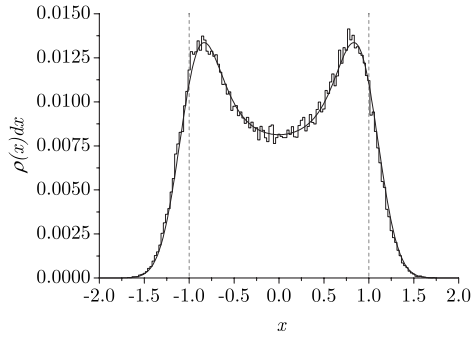

FIG. 4. Empirical probability distribution $\rho(x)dx$ determined from the time series in Fig. 3 (step function) and calculated by convolving ρ_γ and ρ_Γ (thick line). Note that the loci of the poles in $\rho_\gamma(x)$ (marked as dashed vertical lines) do not coincide with the maxima of $\rho(x)$.

$$\gamma(t) = A\cos(\omega t) \tag{13}$$

superimposed with white noise [Gaussian $\rho_\Gamma(x)$]. A realization of the time series $X(t)$ is shown in Fig. 3.

Using Eq. (12)

$$\rho_\gamma(x) = \frac{1}{\pi}\frac{1}{\sqrt{A^2-x^2}} \tag{14}$$

is calculated by dividing $I_t=[0;2\pi]$ into subintervals $I_t^{(1)}=[0;\pi]$ and $I_t^{(2)}=]\pi;2\pi]$ with $\gamma(t)$ being monotone on each $I_t^{(k)}$. Numerical convolution of Eq. (14) and the Gaussian density $\rho_\Gamma(x)$ gives $\rho(x)$ plotted in Fig. 4. This theoretical prediction based on Eqs. (5) and (6) agrees with the probability distribution directly determined from the time series in Fig. 3.

It is evident from Eq. (14) that $\rho_\gamma(x)$ exhibits two singularities at $x=\pm A$ due to the vanishing first derivative at the extrema of $\gamma(t)$. More generally a flat tangent of the trend at some $\tilde{\gamma}$, e.g., caused by reversal points or phases of constant $\gamma(t)$, results in a singularity of $\rho_\gamma(x)$, which can be derived from Eq. (12). As a consequence the global probability density $\rho(x)$ will typically exhibit a local maximum at approximately $x=\tilde{\gamma}$ (see Fig. 4). However, if one wishes to extract information about $\gamma(t)$ from $\rho(x)$, it has to be noted that, as an effect of convolution, the maxima of ρ are not inevitably identical with $\tilde{\gamma}$: In Fig. 4 the maxima are shifted from $\tilde{\gamma}=\pm 1$ to smaller $|x|$, as $\rho_\gamma(x)$ is not symmetric about ± 1.

For 24-h time series of RR intervals the effect of circadian variance can clearly be observed in the well-known bimodal probability distribution: As noted in the introduction the trend can in this case be approximated by a cosine-shaped function or, what will be shown later, by a $\gamma(t)$ being constant during day and night. In both cases $\rho_\gamma(x)$ exhibits two singularities which in turn cause a twice peaked probability distribution.

C. Conditional probability density

The conditional probability density $\rho(\hat{x}|x,\tau)$ for finding some $X(t+\tau)=\hat{x}$ given that its predecessor $X(t)=x$ is defined by

$$\rho(\hat{x}|x,\tau)d\hat{x} = P\{\hat{x} \leqslant X(t+\tau) \leqslant \hat{x} + d\hat{x}|X(t) = x\}. \quad (15)$$

Using the identity

$$\rho(\hat{x}|x,\tau) = \frac{\rho(\hat{x},x|\tau)}{\rho(x)} \quad (16)$$

[27], where $\rho(x)$ is known from Eq. (5), the problem of calculating $\rho(\hat{x}|x,\tau)$ is shifted towards the question how to determine the joint density $\rho(\hat{x},x|\tau)$ for finding t with $X(t)=x$ and $X(t+\tau)=\hat{x}$.

As $\Gamma(t,\tau)$ and $\Gamma(t+\tau,\tau)$ were assumed to be uncorrelated, the joint probability density $\rho(\hat{x},x|\tau,t)$ for fixed t is written as the product of probabilities for two independent processes:

$$\rho(\hat{x},x|\tau,t)d\hat{x}dx = P\{X(t+\tau) \in [\hat{x},\hat{x}+d\hat{x}]|t\} \times P\{X(t) \in [x,x+dx]|t\}. \quad (17)$$

As γ is given by t and $t+\tau$ respectively, the probabilities only depend on the stochastic process Γ. Therefore

$$\rho(\hat{x},x|\tau,t) = \rho_\Gamma[x-\gamma(t)]\rho_\Gamma[\hat{x}-\gamma(t+\tau)]. \quad (18)$$

The global conditional probability density is then calculated by integrating over the whole time series:

$$\rho(\hat{x},x|\tau) = \frac{1}{T-\tau}\int_0^{T-\tau} \rho_\Gamma[x-\gamma(t)]\rho_\Gamma[\hat{x}-\gamma(t+\tau)]dt. \quad (19)$$

We consider the limiting case $\tau \approx 0$, which is valid for all τ with $\gamma(t) \approx \gamma(t+\tau)$. Using this approximation and changing the integration variable from t to γ

$$\begin{aligned}\rho(\hat{x},x|0) &= \frac{1}{T}\int_{\gamma(0)}^{\gamma(T)} \rho_\Gamma[x-\gamma]\rho_\Gamma[\hat{x}-\gamma]\frac{dt}{d\gamma}d\gamma \\ &= \int_{I_\gamma} \rho_\Gamma[x-\gamma]\rho_\Gamma[\hat{x}-\gamma]\frac{1}{T}\left|\frac{1}{(d\gamma/dt)}\right|d\gamma \\ &\overset{(11)}{=} \int_{I_\gamma} \rho_\Gamma[x-\gamma]\rho_\Gamma[\hat{x}-\gamma]\rho_\gamma(\gamma)d\gamma. \end{aligned} \quad (20)$$

Here without loss of generality we assumed monotonically increasing $\gamma(t)$ and used the rule for differentiating the inverse of a function [28]. See Appendix C for the proof of Eq. (20) in the case of general $\gamma(t)$.

IV. STATIONARY TREATMENT OF THE MODEL: THE RECONSTRUCTION OF $g(x)$

Friedrich *et al.* have recently proposed a method for recovering the deterministic term $g(x)$ in Eq. (2) from experimental data [17], if the process under consideration is stationary. Observations based on this algorithm, e.g., number and stability of fixed points, however, are masked by a time dependency of the regulatory mechanism. In view of the wide field of applications indicated in the introduction it seems advisable to demonstrate how to determine the effects of such trends on the shape of $g(x)$ and to calculate this function for some simple cases of $\gamma(t)$, which might serve as a first approximation of general time series.

A. Method of reconstruction

Assuming g and h to be functions of x only, Eq. (2) is averaged over time for all $X(t)=x$, yielding

$$g(x|\tau) = \langle X(t+\tau) - X(t)\rangle_{X(t)=x} = \langle X(t+\tau)\rangle_{X(t)=x} - x, \quad (21)$$

which is stated in Refs. [17,26] for the continuous case [Eq. (1)]. With the notation introduced above Eq. (21) is rewritten

$$g(x|\tau) = \int_{-\infty}^{+\infty} \hat{x}\rho(\hat{x}|x,\tau)d\hat{x} - x \overset{(16)}{=} \frac{1}{\rho(x)}\int_{-\infty}^{+\infty} \hat{x}\rho(\hat{x},x|\tau)d\hat{x} - x. \quad (22)$$

In the limiting case $\tau \approx 0$

$$g(x) := g(x|0) = \frac{1}{\rho(x)}\int_{I_\gamma} s\rho_\Gamma(x-s)\rho_\gamma(s)ds + \int_{-\infty}^{+\infty} s\rho_\Gamma(s)ds - x \quad (23)$$

is obtained (see Appendix D for a proof).[3] If $\rho_\Gamma(x)$ is symmetric around $x=0$ as in the case of Gaussian noise, the second term vanishes.

B. Special cases

The results derived above are applied on simple model trends, which allows one to approximate $\gamma(t)$ underlying empirical data.

1. Piecewise constant trend

A trend

$$\gamma(t) = \sum_k \xi_k \vartheta[I_t^{(k)}](t) \quad (24)$$

(with $\vartheta[J](t)=1$ for $t \in J$ and $=0$ otherwise), which is constant over subintervals $I_t^{(k)}$, gives an associated probability density

$$\rho_\gamma(x) = \sum_k \frac{\|I_t^{(k)}\|}{\|I_t\|}\delta(x-\xi_k). \quad (25)$$

By inserting this equation into Eq. (23)

[3] As we stated above, the approximation $\tau \approx 0$ is valid for all τ that are small compared to the time scale of the trend, i.e., if $\gamma(t) \approx \gamma(t+\tau)\,\forall\, t \in I_t$. This allows one to apply the analysis of $g(x)$ to all $g(x|\tau)$ that are reconstructed by the use of Eq. (21) with an empirical τ that satisfies the given condition. Note that, in particular, $\tau \geqslant 1$ for discrete time series.

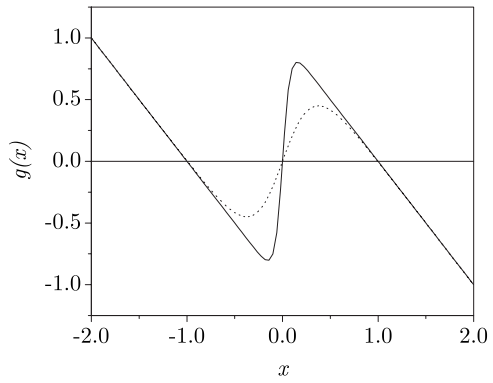

FIG. 5. $g(x)$ as given in Eq. (26) for white noise with $\xi_{1,2}=\pm 1$, $\|I_t^{(1)}\|=\|I_t^{(2)}\|$ and standard deviation $\sigma=0.4$ (continuous line) and $\sigma=0.8$ (dotted line), respectively.

$$g(x)=\frac{\sum_k \xi_k \|I_t^{(k)}\|\rho_\Gamma(x-\xi_k)}{\sum_k \|I_t^{(k)}\|\rho_\Gamma(x-\xi_k)}-x \tag{26}$$

is obtained under the assumption of symmetric $\rho_\Gamma(x)$. $g(x)$ is plotted in Fig. 5 for $k=2$, $\xi_{1,2}=\pm 1$, $\|I_t^{(1)}\|=\|I_t^{(2)}\|$ in the case of white noise with two different standard deviations σ. If the overlap of the $\rho_\gamma(x-\xi_k)$ can be neglected, $g(x)$ is approximated by a straight line with slope -1

$$g(x)=-x+\xi_k \vartheta[U(\xi_k)](x) \tag{27}$$

in some neighborhood $U(\xi_k)$ of ξ_k.

This analysis is confirmed by numerical simulations: By the use of Eq. (21) $g(x|1)$ is computed from a discrete time series subject to the trend

$$\gamma(t)=\begin{cases}-1 & t\in[0,0.3T],\\ +1 & t\in[0.3T,T]\end{cases} \tag{28}$$

with additive white noise (Fig. 6). The two neighborhoods $U(\pm 1)$ can clearly be distinguished, while the relatively small value of σ leads to sharp edge at $x\approx 0$.

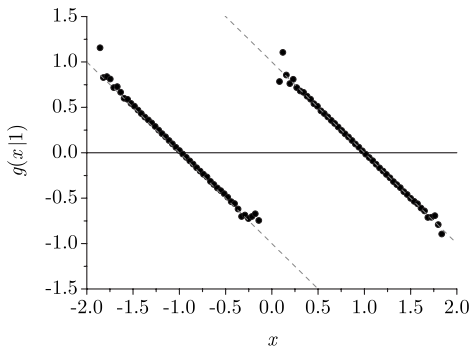

FIG. 6. $g(x|1)$ for the piecewise constant trend given in Eq. (28) superimposed with white noise ($\sigma=0.2$, $T=10^6$, $\tau=1$). According to Eq. (27) two neighborhoods $U(\xi_k)$ with zero crossings at $x=\xi_k$ are observed for $\xi_{1,2}=\pm 1$.

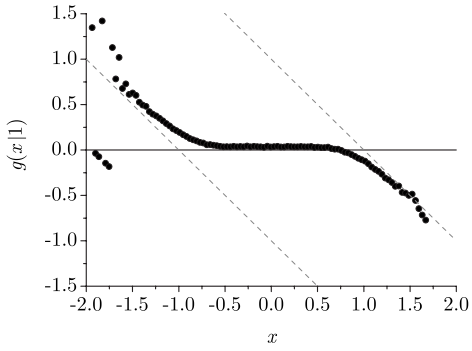

FIG. 7. $g(x|1)$ for the linearly increasing trend given in Eq. (29) superimposed with white noise ($\frac{\|I_\gamma\|}{\|I_t\|}=\frac{2}{T}$, $\gamma_{\min}=-1$, $\sigma=0.2$, $T=10^6$, $\tau=1$). $g(x|1)\approx 0$ around $x=0$ and approaches linear behavior with slope -1 for large enough $|x|$.

2. Linear trend

A linearly increasing trend

$$\gamma(t)=\frac{\|I_\gamma\|}{\|I_t\|}t+\gamma_{\min} \tag{29}$$

has a constant probability density

$$\rho_\gamma(x)=\frac{\|I_t\|}{\|I_\gamma\|}\vartheta[I_\gamma](x). \tag{30}$$

Inserting this in Eq. (23) gives

$$g(x)=\frac{\int_{I_\gamma}\gamma\rho_\Gamma(x-\gamma)d\gamma}{\int_{I_\gamma}\rho_\Gamma(x-\gamma)d\gamma}-x \tag{31}$$

for symmetric $\rho_\Gamma(x)$.

If $\rho_\Gamma(x)$ is concentrated on some interval $I_\Gamma=[-\epsilon,\epsilon]$ and $x\in[\gamma_{\min}+\epsilon,\gamma_{\max}-\epsilon]$, then g vanishes, as can be seen in Fig.

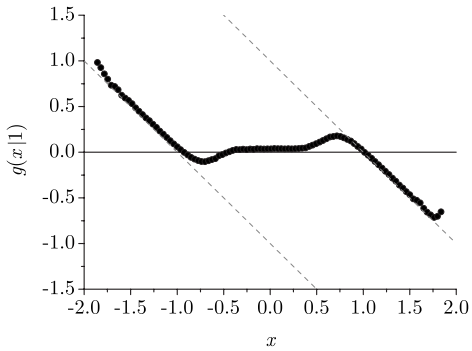

FIG. 8. $g(x|1)$ for the trend given in Eq. (32) superimposed with white noise ($\sigma=0.2$, $T=10^6$, $\tau=1$). x values at approximately 0 will mostly be found in the transitional phase of the time series, so that $g(x|1)$ coincides with g from Fig. 7 at $x\approx 0$. The linear phases with slope -1 and zero crossings at $x\approx\pm 1$, however, are due to the constant sections of $\gamma(t)$ with $\xi_{1,2}=\pm 1$.

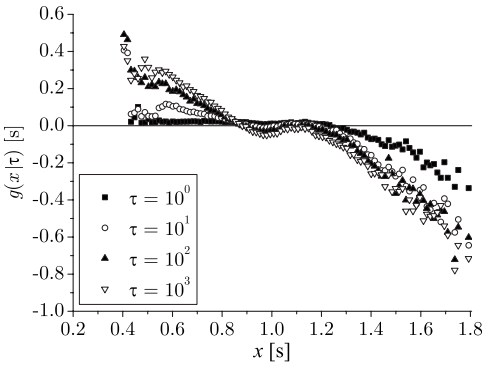

FIG. 9. $g(x|\tau)$ for the RR interval time series in Fig. 1. The two stability points at $x \approx 0.85$ and 1.1 s correspond to the averages of day and night phases, respectively. $g(x|\tau)$ flattens for decreasing τ due to correlations between successive heart beats.

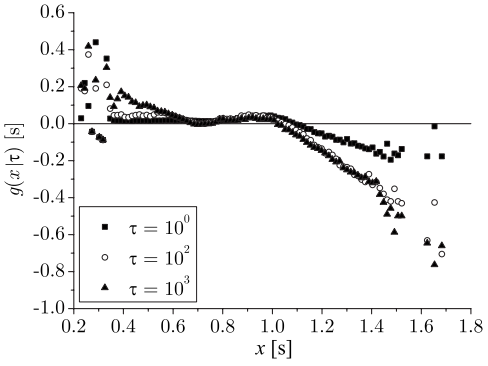

FIG. 10. $g(x|\tau)$ for the RR interval time series in Fig. 2. $g(x|\tau)$ exhibits a relatively flat region between the two stability nodes at $x \approx 0.7$ and 1.1 s due to the distinct transitional phase in the time series.

7. For large enough $|x|$, g approaches linear behavior with slope -1 (see Appendix E for the proofs of the given results).

3. Piecewise constant trend with transitional phase

Empirical data is in a first approximation described as governed by a piecewise constant or linearly monotone $\gamma(t)$ as analyzed in the last two paragraphs. The combination of these two models describes constant phases as defined in Eq. (24), which are connected by a linear transition period analogous to Eq. (29). Figure 8 shows $g(x|1)$ for the trend

$$\gamma(t) = \begin{cases} -1, & t \in [0,0.3T], \\ -1 + \dfrac{2t}{0.4T}, & t \in [0.3T,0.7T], \\ +1, & t \in [0.7T,T] \end{cases} \tag{32}$$

with additive white noise. For $|x| > 1$ the same behavior as in Fig. 6 is observed: Decreasing g with slope -1. For $x \approx 0$ in contrast the function is dominated by the transitional period: g is flattened between the two zero crossings. This effect is similar to the case, in which the standard deviation σ of the stochastic process $\Gamma(t,\tau)$ is increased (see Fig. 5).

C. Application to physiological data

Application of the method of reconstruction described above on 24-h time series of RR intervals has recently shown an n-stable deterministic force $g(x|\tau)$, where n typically equals to 2 [20,21]. Thereby a stable node was constituted by a zero crossing with negative slope. This observation is supported by our own data analysis, examples of which are displayed in Figs. 9 and 10.

For large enough time delay τ, $g(x|\tau)$ bears resemblance to our simulations in Figs. 5 and 8. This similarity is ascribed to the fact that the physiological data in Figs. 1 and 2 show significant differences in heart rate between day and night phases and therefore are in a first approximation modeled as being governed by a piecewise constant trend. Thus each phase of steady physical stress leads to a stable fixed point in g; particularly a distinct circadian variation implies, beside a bimodal probability distribution as seen in the last section, bistability in regard to the deterministic part of the Langevin equation.

The region of $g(x|\tau)$ in Figs. 9 and 10 between two stable fixed points is determined both by the standard deviation of the noise source and by the transition between the phases: As was shown above, g is flattened by increasing σ (Fig. 5) and by a long interval of strictly monotone $\gamma(t)$ (Figs. 6–8). Kuusela [21] indicates that such a plateau phase in the reconstructed g is characteristic for patients suffering of congestive heart failure. For this observation potential explanations are offered by the two effects mentioned: The deteriorated performance of the cardiovascular system might result in decelerated adaptation mechanisms and thus longer transitional phases. Simultaneously the two fixed points will draw nearer due to the reduced activity of the patient, which will raise, in spite of the decreased absolute heart rate variability [29–31], the relative value of σ. A decision on which explanation accounts for the differences between CHF patients and reference group is to be based on a careful analysis of the respective time series.

In the discussion above we have used the results that we derived from our model under the assumption of $\tau \approx 0$. Indeed the time delays used in Figs. 9 and 10 are small compared to the lengths of phases with constant $\gamma(t)$, which last $>10^4$ beats. However, $g(x|\tau)$ exhibits a τ dependency, where the predictions from our model are best met at delays $>10^2$ beats, while g flattens for decreasing τ. This results from correlations between successive heart beats including respiration and adaptation to environmental influences varying on time scales of seconds and minutes. Only if the parts of the signal that are modeled to be stochastic [Eq. (4)] are decorrelated, the assumption for Eq. (18) holds and the derived predictions are valid. Note that our predictions also fail, when τ is too large and $\gamma(t+\tau) \approx \gamma(t)$ does not hold any more: A time delay comparable to the lengths of the constant phases conceals circadian variation and instead suggests a stationary regulatory mechanism towards mean heart rate.

Our hypothesis, that bistability in g is caused by circadian variation, can be tested by applying the reconstruction algorithm to day and night phases of the time series separately: The sequence of RR intervals of Fig. 1 is split up into three parts as shown in Fig. 11. The associated $g(x|\tau)$ graphs are

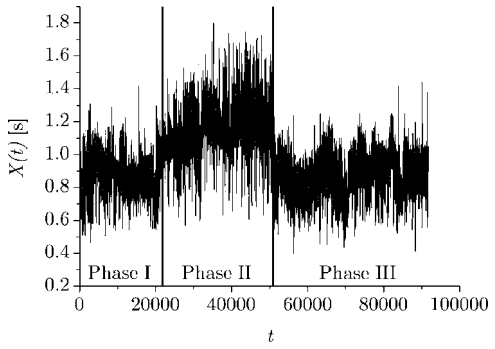

FIG. 11. 24-h time series of RR intervals $X(t)$ over beat number t as seen in Fig. 1. Day and night phases are separated by vertical lines.

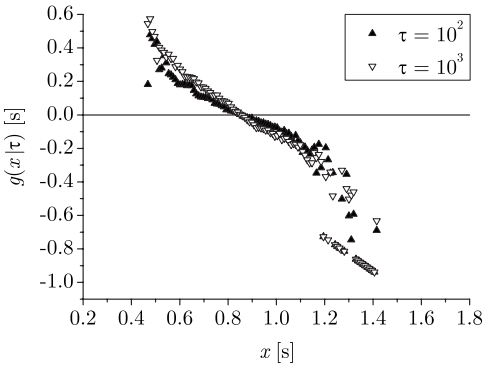

FIG. 12. $g(x|\tau)$ for phase I as given in Fig. 11 with $\tau=10^2$ and 10^3. A single stable fixed point at $x\approx 0.85$ s is detected, corresponding to the leftmost zero crossing in Fig. 9.

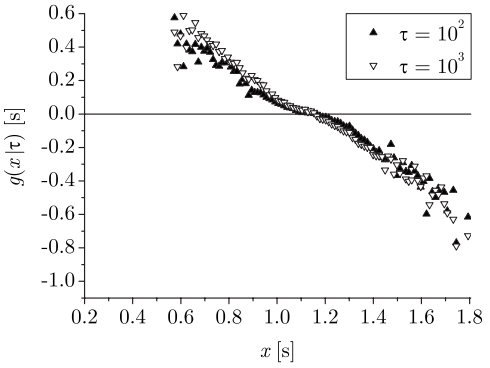

FIG. 13. $g(x|\tau)$ for phase II as given in Fig. 11 ($\tau=10^2$ and 10^3), exhibiting a single stable fixed point at $x\approx 1.15$ s.

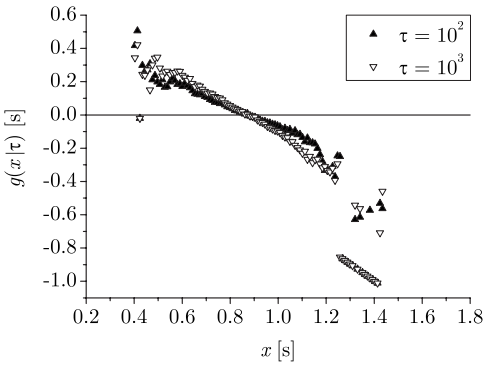

FIG. 14. $g(x|\tau)$ for phase III as given in Fig. 11 ($\tau=10^2$ and 10^3), exhibiting a single stable fixed point at $x\approx 0.85$ s.

given in Figs. 12–14 for $\tau=10^2$ and 10^3. All of them are characterized by monostable behavior with a fixed point at $x\approx 0.85$ s (phases I and III) and 1.15 s (phase II), respectively. These values perfectly agree with those of the bistable $g(x|\tau)$ in Fig. 9, the shape of which is thus the result of the concatenation of the three stationary phases I-III to one single time series with a nonconstant trend.

Figures 12–14 match the observations of Ghasemi *et al.* [22], who also found linear $g(x|1)$ in 6-h time series, at least in the case of healthy patients. For persons suffering from congestive heart failure, however, a flat cubic dependence on x was suggested for the deterministic force. We suppose that these observations, which differ from the predictions derived from our model, are to be ascribed to the correlations present in the time series: As discussed above for Figs. 9 and 10, $g(x|\tau)$ flattens for decreasing τ, i.e., if the delay parameter approaches the correlation time. As Ghasemi and co-workers set $\tau=1$, their calculations are performed within the range of correlations, which they indicate themselves by determining the Markov time scale. The latter is significantly increased in CHF patients, which explains the deviations from our model, which comprises δ-correlated noise only.

The Langevin equation under study hence describes processes, for which values of the empirical delay parameter τ can be found, which are much larger than the correlation time of the data and yet negligible in comparison to the time scale of the trend. In the range of such adequate τ, however, the stable nodes of $g(x|\tau)$ become independent of the time delay and indicate ξ_i in case of a piecewise constant trend. As an application in cardiology, this offers the possibility to calculate mean heart rate of day and night phases, respectively, and thus to determine the range of these two stationary phases independently of potentially erroneous information such as diaries and markers.

V. SUMMARY

In this article the statistical properties of a stochastic process subject to a nonstationary regulatory mechanism have been analyzed: Global and conditional probability densities, as well as the moments of the distribution were derived and applied on several simple model systems. These results were used to explain observations recently made for RR interval

time series: Both a polymodal probability distribution and polystability displayed in the deterministic term of the Langevin equation were in a mathematically stringent way traced back to a common cause, phases of different physical stress, especially circadian variation. Moreover we offered explanations for the differences in the shape of g between CHF patients and the reference group of healthy subjects.

ACKNOWLEDGMENTS

We thank Jörg O. Schwab from University of Bonn, Department of Medicine (Cardiology), for providing the 24-h time series of ECG data that we used for demonstration.

APPENDIX A: DERIVATION OF EQ. (10)

Equation (7) defines the moments of X

$$\langle X^n\rangle = \int_{-\infty}^{\infty} x^n \rho(x)dx \overset{(5),(6)}{=} \int_{-\infty}^{\infty} x^n \int_{-\infty}^{\infty} \rho_\gamma(s)\rho_\Gamma(x-s)dsdx$$

$$\overset{u:=x-s}{=} \int_{-\infty}^{\infty} \rho_\gamma(s) \int_{-\infty}^{\infty} (u+s)^n \rho_\Gamma(u)duds.$$

Expanding the term $(u+s)^n$ [28] gives

$$\langle X^n\rangle = \sum_{k=0}^{n} \binom{n}{k} \int_{-\infty}^{\infty} s^k \rho_\gamma(s)ds \int_{-\infty}^{\infty} u^{n-k}\rho_\Gamma(u)du$$

$$\overset{(8),(9)}{=} \sum_{k=0}^{n} \binom{n}{k} \langle\gamma^k\rangle\langle\Gamma^{n-k}\rangle$$

in accordance with Eq. (10). ■

APPENDIX B: DERIVATION OF EQS. (11) and (12)

In the first instance $\gamma(t)$ is confined to be strictly increasing. For an infinitesimally small interval $[x,x+dx]$

$$\rho_\gamma(x)dx = P\{x \leqslant \gamma(t) \leqslant x+dx\}$$
$$= P\{\gamma^{-1}(x) \leqslant t \leqslant \gamma^{-1}(x+dx)\}.$$

The probability is thus given by the length of the interval $[\gamma^{-1}(x), \gamma^{-1}(x+dx)]$ relative to the whole duration $\|I_t\|$ of the measurement.

$$\rho_\gamma(x)dx = \frac{|\gamma^{-1}(x+dx) - \gamma^{-1}(x)|}{\|I_t\|}. \tag{B1}$$

Expanding $\gamma^{-1}(x+dx)$ around x

$$\gamma^{-1}(x+dx) = \gamma^{-1}(x) + \left[\frac{d}{ds}\gamma^{-1}(s)\right]_{s=x} dx$$

gives

$$\rho_\gamma(x)dx = \frac{1}{\|I_t\|}\left|\left[\frac{d}{ds}\gamma^{-1}(s)\right]_{s=x}\right| dx,$$

which is Eq. (11). ■

For general $\gamma(t)$ the sampling interval I_t is split up into K subintervals $I_t^{(k)}$ such that $\gamma(t)$ is monotone on each $I_t^{(k)}$; hence the inverse exists and is denoted as $\gamma_k^{-1}(x)$ for every $I_t^{(k)}$. Equation (B1) is then substituted by

$$\rho_\gamma(x)dx = \sum_{k:x\in I_t^{(k)}} \frac{|\gamma_k^{-1}(x+dx) - \gamma_k^{-1}(x)|}{\|I_t\|}.$$

Accordingly Eq. (12) is obtained. ■

APPENDIX C: PROOF OF EQ. (20)

The conditional probability density $\rho(\hat{x},x|\tau)$ is considered in the limiting case $\tau\approx 0$.

$$\rho(\hat{x},x|0) \overset{(19)}{=} \frac{1}{\|I_t\|}\int_{I_t} \rho_\Gamma[x-\gamma(t)]\rho_\Gamma[\hat{x}-\gamma(t)]dt.$$

In the same way as in Appendix B the interval I_t is decomposed into K subintervals $I_t^{(k)}=[t_{k-1},t_k[$ with time steps $t_0 < t_1 < \cdots < t_{K-1} < t_K$ such that $\gamma(t)$ is monotone on each $I_t^{(k)}$. Thus

$$\rho(\hat{x},x|0) = \frac{1}{\|I_t\|}\sum_{k=1}^{K}\int_{t_{k-1}}^{t_k} \rho_\Gamma[x-\gamma(t)]\rho_\Gamma[\hat{x}-\gamma(t)]dt.$$

With $\gamma(t)$ being piecewise surjective the integration variable is changed from t to γ

$$\rho(\hat{x},x|0) = \sum_{k=1}^{K}\int_{\gamma(t_{k-1})}^{\gamma(t_k)} \rho_\Gamma(x-\gamma)\rho_\Gamma(\hat{x}-\gamma)\frac{1}{\|I_t\|}\frac{dt}{d\gamma}d\gamma$$

$$= \sum_{k=1}^{K}\int_{\gamma(I_t^{(k)})} \rho_\Gamma(x-\gamma)\rho_\Gamma(\hat{x}-\gamma)\frac{1}{\|I_t\|}\left|\frac{dt}{d\gamma}\right| d\gamma$$

$$= \int_{\gamma(I_t)} \rho_\Gamma(x-\gamma)\rho_\Gamma(\hat{x}-\gamma)\frac{1}{\|I_t\|}\sum_{k:\gamma\in\gamma(I_t^{(k)})}\left|\frac{1}{(d\gamma/dt)}\right| d\gamma$$

$$= \int_{I_\gamma} \rho_\Gamma(x-\gamma)\rho_\Gamma(\hat{x}-\gamma) \times \frac{1}{\|I_t\|}\sum_{k:\gamma\in(I_\gamma^{(k)})}\left|\left[\frac{d}{ds}\gamma_k^{-1}(s)\right]_{s=\gamma}\right| d\gamma$$

$$\overset{(12)}{=} \int_{I_\gamma} \rho_\Gamma(\hat{x}-\gamma)\rho_\Gamma(x-\gamma)\rho_\gamma(\gamma)d\gamma.$$

As above $\gamma_k^{-1}(x)$ denotes the inverse of $\gamma(t)$ on the subinterval $I_t^{(k)}$. ■

APPENDIX D: PROOF OF EQ. (23)

Assuming $\tau\approx 0$

$$
\begin{aligned}
g(x) + x &\overset{(22)}{=} \frac{1}{\rho(x)} \int_{-\infty}^{+\infty} \hat{x}\rho(\hat{x},x|0)d\hat{x} \\
&\overset{(20)}{=} \frac{1}{\rho(x)} \int_{-\infty}^{+\infty} \hat{x} \int_{I_\gamma} \rho_\Gamma(x-\gamma)\rho_\Gamma(\hat{x}-\gamma)\rho_\gamma(\gamma)d\gamma d\hat{x} \\
&= \frac{1}{\rho(x)} \int_{I_\gamma} \rho_\Gamma(x-\gamma)\rho_\gamma(\gamma) \int_{-\infty}^{+\infty} \hat{x}\rho_\Gamma(\hat{x}-\gamma)d\hat{x}d\gamma \\
&\overset{s:=\hat{x}-\gamma}{=} \frac{1}{\rho(x)} \int_{I_\gamma} \rho_\Gamma(x-\gamma)\rho_\gamma(\gamma) \\
&\quad \times \left[\int_{-\infty}^{+\infty} s\rho_\Gamma(s)ds + \gamma \int_{-\infty}^{+\infty} \rho_\Gamma(s)ds \right] d\gamma \\
&\overset{(5)}{=} \int_{-\infty}^{+\infty} s\rho_\Gamma(s)ds + \frac{1}{\rho(x)} \int_{I_\gamma} \rho_\Gamma(x-\gamma)\rho_\gamma(\gamma)\gamma d\gamma,
\end{aligned}
$$

which is Eq. (23). ■

APPENDIX E: $g(x)$ IN CASE OF A LINEAR TREND

The function $g(x)$ is calculated for $\gamma(t)$ as given in Eq. (29). Assuming symmetric $\rho_\Gamma(x)$

$$
g(x) + x \overset{(23)}{=} \frac{1}{\rho(x)} \int_{I_\gamma} s\rho_\Gamma(x-s)\rho_\gamma(s)ds.
$$

The denominator is

$$
\begin{aligned}
\rho(x) &\overset{(5),(6)}{=} \int_{-\infty}^{\infty} \rho_\gamma(s)\rho_\Gamma(x-s)ds \\
&\overset{(30)}{=} \int_{-\infty}^{\infty} \frac{\|I_t\|}{\|I_\gamma\|} \vartheta[I_\gamma](x)\rho_\Gamma(x-s)ds \\
&= \frac{\|I_t\|}{\|I_\gamma\|} \int_{I_\gamma} \rho_\Gamma(x-s)ds.
\end{aligned}
$$

The numerator is calculated as

$$
\begin{aligned}
\int_{I_\gamma} s\rho_\Gamma(x-s)\rho_\gamma(s)ds &\overset{(30)}{=} \int_{I_\gamma} s\rho_\Gamma(x-s)\frac{\|I_t\|}{\|I_\gamma\|}\vartheta[I_\gamma](s)ds \\
&= \frac{\|I_t\|}{\|I_\gamma\|} \int_{I_\gamma} s\rho_\Gamma(x-s)ds.
\end{aligned}
$$

Thus

$$
g(x) = \frac{\int_{I_\gamma} s\rho_\Gamma(x-s)ds}{\int_{I_\gamma} \rho_\Gamma(x-s)ds} - x
$$

as suggested in Eq. (31). ■

Substituting u for $x-s$ gives

$$
g(x) = \frac{x\int_{I_u} \rho_\Gamma(u)du - \int_{I_u} u\rho_\Gamma(u)du}{\int_{I_u} \rho_\Gamma(u)du} - x = -\frac{\int_{I_u} u\rho_\Gamma(u)du}{\int_{I_u} \rho_\Gamma(u)du}
$$

with $I_u=[x-\gamma_{\max},x-\gamma_{\min}]$.

We now consider the special case, in which $\rho_\Gamma(x)$ is concentrated on some interval I_Γ in such way that $\rho_\Gamma(x)\approx 0$ if $x \notin I_\Gamma$. Then two limiting cases can be analyzed: First, if $I_\Gamma \subseteq I_u$,

$$
g(x) \approx -\frac{\int_{I_\Gamma} u\rho_\Gamma(u)du}{\int_{I_\Gamma} \rho_\Gamma(u)du} = -\int_{I_\Gamma} u\rho_\Gamma(u)du
$$

and vanishes due to the symmetry of $\rho_\Gamma(u)$. ■

Second, if $I_\Gamma \cap I_u = \emptyset$, l'Hospital's rule is used to approximate $g(x)$.

$$
\begin{aligned}
g(x) &= -\frac{\frac{\partial}{\partial x}\int_{x-\gamma_{\max}}^{x-\gamma_{\min}} u\rho_\Gamma(u)du}{\frac{\partial}{\partial x}\int_{x-\gamma_{\max}}^{x-\gamma_{\min}} \rho_\Gamma(u)du} \\
&= -\frac{[u\rho_\Gamma(u)]_{u=x-\gamma_{\min}} - [u\rho_\Gamma(u)]_{u=x-\gamma_{\max}}}{[\rho_\Gamma(u)]_{u=x-\gamma_{\min}} - [\rho_\Gamma(u)]_{u=x-\gamma_{\max}}},
\end{aligned}
$$

where the rule for differentiating a parameter integral [28] has been applied.

If $\rho_\Gamma(x-\gamma_{\min}) \gg \rho_\Gamma(x-\gamma_{\max})$ (e.g., for white noise and $x < \gamma_{\min}$), $g(x)$ is written as

$$
g(x) = -\frac{(x-\gamma_{\min})\rho_\Gamma(x-\gamma_{\min})}{\rho_\Gamma(x-\gamma_{\min})} = -x + \gamma_{\min}
$$

and for $\rho_\Gamma(x-\gamma_{\min}) \ll \rho_\Gamma(x-\gamma_{\max})$

$$
g(x) = -x + \gamma_{\max}.
$$

Hence, if x is sufficiently far from I_γ, i.e., if $x \notin I_\gamma$ is such that the given requirements are fulfilled, then $g(x)$ converges to linear decrease with slope -1. ■

[1] H. Huikuri, K. Kessler, E. Terracall, A. Castellanos, M. Linnaluoto, and R. Myerburg, Am. J. Cardiol. **65**, 391 (1990).
[2] G. Panina, U. N. Khot, E. Nunziata, R. J. Cody, and P. F. Binkley, Am. Heart J. **129**, 748 (1995).
[3] W. Nelson, Y. L. Tong, J. Lee, and F. Halberg, Chronobiologia **6**, 305 (1979).
[4] J. Fernández and R. Hermida, Chronobiol Int. **15**, 191 (1998).
[5] P. Langevin, C. R. Acad. Sci. **146**, 530 (1908).
[6] K. Lindenberg and B. J. West, *The Nonequilibrium Statistical Mechanics of Open and Closed Systems* (VCH, New York, 1990).
[7] R. Kubo, M. Toda, and N. Hashitsume, *Statistical Physics II. Nonequilibrium Statistical Mechanics*, Springer Series in Solid-State Sciences (Springer, Berlin, 1991).
[8] N. G. van Kampen, *Stochastic Processes in Physics and Chemistry* (North-Holland, Amsterdam, 1992).
[9] K. Itô, Nagoya Math. J. **1**, 35 (1950).
[10] R. L. Stratonovich, SIAM J. Control **4**, 362 (1966).
[11] M. Lax, Rev. Mod. Phys. **38**, 541 (1966).
[12] R. Zwanzig, Phys. Rev. **124**, 983 (1961).
[13] H. Mori, Prog. Theor. Phys. **33**, 423 (1965).
[14] R. Kubo, Rep. Prog. Phys. **29**, 255 (1966).
[15] R. F. Fox, J. Stat. Phys. **16**, 259 (1977).
[16] S. Siegert, R. Friedrich, and J. Peinke, Phys. Lett. A **243**, 275 (1998).
[17] R. Friedrich, S. Siegert, J. Peinke, S. Lück, M. Siefert, M. Lindemann, J. Raethjen, G. Deuschl, and G. Pfister, Phys. Lett. A **271**, 217 (2000).
[18] J. Gradišek, I. Grabec, S. Siegert, and R. Friedrich, J. Sound Vib. **252**, 545 (2002).
[19] J. Gradišek, E. Govekar, and I. Grabec, J. Sound Vib. **252**, 563 (2002).
[20] T. Kuusela, T. Shepherd, and J. Hietarinta, Phys. Rev. E **67**, 061904 (2003).
[21] T. Kuusela, Phys. Rev. E **69**, 031916 (2004).
[22] F. Ghasemi, J. Peinke, M. Sahimi, and M. R. Rahimi Tabar, Eur. Phys. J. B **47**, 411 (2005).
[23] C.-K. Peng, S. Havlin, H. E. Stanley, and A. L. Goldberger, Chaos **5**, 82 (1995).
[24] P. Bernaola-Galván, P. C. Ivanov, L. A. Nunes Amaral, and H. E. Stanley, Phys. Rev. Lett. **87**, 168105 (2001).
[25] F. Ghasemi, M. Sahimi, J. Peinke, and M. R. R. Tabar, J. Biol. Phys. **32**, 117 (2006).
[26] H. Risken, *The Fokker-Planck Equation* (Springer, Berlin, 1989).
[27] P. G. Hoel, S. C. Port, and C. J. Stone, *Introduction to Probability Theory* (Houghton Mifflin Company, Boston, 1971).
[28] I. N. Bronshtein and Semendyayew, *Handbook of Mathematics* (Springer, Berlin, 1998).
[29] R. Kleiger, J. Miller, J. Bigger, and A. Moss, Am. J. Cardiol. **59**, 256 (1987).
[30] J. Nolan *et al.*, Circulation **98**, 1510 (1998).
[31] P. Ponikowski *et al.*, Am. J. Cardiol. **79**, 1645 (1997).